Am J Physiol Gastrointest Liver Physiol 309: G826–G840, 2015.
First published September 3, 2015; doi:10.1152/ajpgi.00041.2015.

The p66^{Shc} protein controls redox signaling and oxidation-dependent DNA damage in human liver cells

Sebastio Perrini,[1] Federica Tortosa,[1] Annalisa Natalicchio,[1] Consiglia Pacelli,[2] Angelo Cignarelli,[1] Vincenzo O. Palmieri,[3] Cristina Caccioppoli, Francesca De Stefano,[1] Stefania Porro,[1] Anna Leonardini,[1] Romina Ficarella,[1] Michele De Fazio,[4] Tiziana Cocco,[2] Francesco Puglisi,[4,5] Luigi Laviola,[1] Giuseppe Palasciano,[3] and Francesco Giorgino[1]

[1]*Department of Emergency and Organ Transplantation, Section on Internal Medicine, Endocrinology, Andrology and Metabolic Diseases, University of Bari Aldo Moro, Bari, Italy;* [2]*Department of Medical Biochemistry, Biology and Physics, University of Bari Aldo Moro, Bari, Italy;* [3]*Department of Biochemical Sciences and Human Oncology, Clinica Medica "A. Murri," University of Bari Aldo Moro, Bari, Italy;* [4]*Department of Emergency and Organ Transplantation, General Surgery and Liver Transplantation, University of Bari Aldo Moro, Bari, Italy; and* [5]*Azienda Sanitaria Locale Bari, Ospedale M. Sarcone, Terlizzi (BA), Italy*

Submitted 16 February 2015; accepted in final form 4 August 2015

Perrini S, Tortosa F, Natalicchio A, Pacelli C, Cignarelli A, Palmieri VO, Caccioppoli C, De Stefano F, Porro S, Leonardini A, Ficarella R, De Fazio M, Cocco T, Puglisi F, Laviola L, Palasciano G, Giorgino F. The p66^{Shc} protein controls redox signaling and oxidation-dependent DNA damage in human liver cells. *Am J Physiol Gastrointest Liver Physiol* 309: G826–G840, 2015. First published September 3, 2015; doi:10.1152/ajpgi.00041.2015.—The p66^{Shc} protein mediates oxidative stress-related injury in multiple tissues. Steatohepatitis is characterized by enhanced oxidative stress-mediated cell damage. The role of p66^{Shc} in redox signaling was investigated in human liver cells and alcoholic steatohepatitis. HepG2 cells with overexpression of wild-type or mutant p66^{Shc}, with Ser^{36} replacement by Ala, were obtained through infection with recombinant adenoviruses. Reactive oxygen species and oxidation-dependent DNA damage were assessed by measuring dihydroethidium oxidation and 8-hydroxy-2′-deoxyguanosine accumulation into DNA, respectively. mRNA and protein levels of signaling intermediates were evaluated in HepG2 cells and liver biopsies from control and alcoholic steatohepatitis subjects. Exposure to H_2O_2 increased reactive oxygen species and phosphorylation of p66^{Shc} on Ser^{36} in HepG2 cells. Overexpression of p66^{Shc} promoted reactive oxygen species synthesis and oxidation-dependent DNA damage, which were further enhanced by H_2O_2. p66^{Shc} activation also resulted in increased Erk-1/2, Akt, and FoxO3a phosphorylation. Blocking of Erk-1/2 activation inhibited p66^{Shc} phosphorylation on Ser^{36}. Increased p66^{Shc} expression was associated with reduced mRNA levels of antioxidant molecules, such as NF-E2-related factor 2 and its target genes. In contrast, overexpression of the phosphorylation defective p66^{Shc} Ala^{36} mutant inhibited p66^{Shc} signaling, enhanced antioxidant genes, and suppressed reactive oxygen species and oxidation-dependent DNA damage. Increased p66^{Shc} protein levels and Akt phosphorylation were observed in liver biopsies from alcoholic steatohepatitis compared with control subjects. In human alcoholic steatohepatitis, increased hepatocyte p66^{Shc} protein levels may enhance susceptibility to DNA damage by oxidative stress by promoting reactive oxygen species synthesis and repressing antioxidant pathways.

oxidative stress; p66^{Shc}; hepatocyte; Akt; FoxO3a; alcoholic steatohepatitis; *Nrf2*

ABERRANT PRODUCTION OF REACTIVE oxygen species (ROS) has been recognized as a major determinant of DNA damage, leading to disruption of tissue homeostasis, organ dysfunction, and onset of chronic degenerative disorders (24, 27, 30). p66^{Shc} has recently emerged as a master regulator of ROS production and a critical intracellular switch conveying oxidative stress signals to DNA damage in multiple cells and tissues, including the vascular wall and heart (11), kidney (29), osteoblasts (1), lymphocytes (25), and hepatocytes (10).

Rodents with genetic deletion of *p66^{Shc}* demonstrate a prolonged life span due to significant resistance to oxidative stress (3, 21, 32) p66$^{Shc-/-}$ mice are also protected against experimental diabetic glomerulopathy (19), diabetic cardiomyopathy, and hyperglycemia-induced endothelial dysfunction and atherogenesis (36), confirming that p66^{Shc} mediates oxidative stress-dependent tissue damage. Furthermore, phosphorylation of p66^{Shc} on Ser^{36} has been identified as the key signaling event mediating p66^{Shc} activation and promotion of its downstream cellular effects (21). In the liver, the levels of total and Ser^{36}-phosphorylated p66^{Shc} protein were found to be significantly augmented in the mouse nonalcoholic steatohepatitis (NASH) model (31). Conversely, ethanol-induced oxidative stress was found to be attenuated in the liver of p66$^{Shc-/-}$ mice (12), suggesting that p66^{Shc} may be involved in the hepatocyte damage in response to metabolic injuries. In addition, ablation of *p66^{shc}* gene in mouse hepatocytes suppressed cellular apoptosis and ROS production after hypoxia/reoxygenation through upregulation of Mn superoxide dismutase (*SOD*) and redox factor-1 (13).

Normally, cells adapt to increased ROS levels by upregulating antioxidant genes (24, 30) and neutralizing ROS through the low-molecular weight antioxidant and phase II detoxifying enzymes (2, 35). The NF-E2-related factor 2 (*Nrf2*) is a master gene involved in the regulation of phase II and antioxidant enzymes [e.g., glutathione *S*-transferase alpha 5 (*GSTA5*), glutathione *S*-transferase muscle 2 (*GSTM2*), and *MnSOD*] (2, 15). Reduced expression of cardiac *Nrf2* was indeed associated with significant increase in nitrosative DNA damage (5). In hepatocytes, *Nrf2* was shown to be required for cell survival during liver development, its deficiency resulting in enhanced oxidative stress both in the normal and injured liver (4). While the detoxifying and ROS-scavenging role of *Nrf2* has been

Address for reprint requests and other correspondence: F. Giorgino, Dept. of Emergency and Organ Transplantation-Section of Internal Medicine, Endocrinology Andrology and Metabolic Diseases, Univ. of Bari Aldo Moro, Piazza Giulio Cesare, 11, I-70124 Bari, Italy (e-mail: francesco.giorgino@uniba.it).

recognized in multiple cytoprotective activities (4, 15, 35), the relationship between p66^{Shc} and *Nrf2* has not been explored.

In this study, we show that p66^{Shc} protein expression is increased in human alcoholic steatohepatitis (ASH) and that in human liver cells p66^{Shc} controls intracellular ROS levels, the antioxidant *Nrf2* and Forkhead box protein O3a (FoxO3a) pathways, and the extent of oxidative DNA damage.

MATERIALS AND METHODS

Antibodies and reagents. Anti-Shc monoclonal antibody was from BD Transduction Laboratories (Lexington, KY). Anti-Shc/p66 (pSer^{36}) antibody was from Calbiochem (Darmstadt, Germany). Anti-MAP kinase (ERK-1/2) antibodies were obtained from Zymed Laboratories (San Francisco, CA). Anti-GAPDH antibody (FL-335) was from Santa Cruz Biotechnology (Santa Cruz, CA). Phospho-Akt (Ser^{473}), total Akt, phospho-p42/p44 MAP kinase (Thr^{202}/Tyr^{204}), phospho-FoxO1a(Thr^{24})/FoxO3a(Thr^{32}), total FoxO3a, phosphorylated Thr^{183}/Tyr^{185}-SAPK/JNK, total SAPK/JNK, phosphorylated Thr^{180}/Tyr^{182}-p38 MAPK, and total p38 MAPK antibodies were purchased from Cell Signaling Technology (Beverly, MA). The MEK inhibitor U0126 was obtained from Calbiochem (La Jolla, CA). Anti-8-oxoguanine monoclonal antibody was purchased from Millipore (MAB3560; Millipore, Billerica, MA). Alexa Fluor^{546} anti-rabbit antibody and the fluorescent dye dihydroethidium (DHE) were obtained from Invitrogen (Invitrogen, Carlsbad, CA). H_2O_2 was from Sigma Aldrich (St. Louis, MO).

Cell cultures. HepG2 human hepatoma cells were from American Type Culture Collection (Rockville, MD) and were cultured in MEM supplemented with 10% FCS (both from GIBCO, Invitrogen, Paisley, UK), 100 U/ml penicillin, 100 mg/ml streptomycin (Lonza, Iquique, Chile), and nonessential amino acids (NEA; GIBCO, Invitrogen).

Adenoviral transfection studies. The recombinant adenoviruses were generated by cloning either the wild-type p66^{Shc}-encoding cDNA or the Ala^{36} p66^{Shc} mutant into the shuttle vector pAdTrack-CMV, containing a green fluorescent protein epitope. Adenovirus production and cells infection were performed as previously described (18, 23).

Immunoblotting analysis. Cell lysate preparation and immunoblotting analysis were performed as previously described (22, 23). Briefly, HepG2 cells mechanically detached in ice-cold lysis buffer, containing 50 mM HEPES pH 7.5, 150 mM NaCl, 1 mM $MgCl_2$, 1 mM $CaCl_2$, 4 mM EDTA, 1% Triton X-100, 10% glycerol, 50 mM NaF, and 10 mM NaPP, supplemented with 100 μM PMSF, 5 ng/ml leupeptin, 1 μg/ml aprotinin, and 2 mM Na_3VO_4. Cell lysates were cleared by centrifugation. Protein concentration was determined by the Bradford assay (Bio-Rad, Hercules, CA), and equal protein samples (60 μg) were separated on 7%−10% SDS-PAGE gels, as appropriate, and electrotransferred onto Hybond-P polyvinylidene difluoride filters (Amersham Life Science, Arlington Heights, IL). The filters were then probed with the specific primary antibodies, and the immunoreactive bands were visualized with horseradish peroxidase-conjugated goat anti-mouse or anti-rabbit IgG (H+L) (Bio-Rad), as appropriate, using an ECL Plus Immunoblotting Detection System (Amersham Life Science), and quantified by densitometric analysis using the Versadoc imaging system (Bio-Rad).

Immunofluorescence analysis of FoxO3a. To visualize FoxO3a translocation, immunofluorescence analysis was performed, as previously described (7). Briefly, HepG2 cells were grown on coverslips in complete medium for the indicated times, then fixed with 3.7% formaldehyde at room temperature for 45 min, and permeabilized at room temperature with 0.1% Triton X-100. Subsequently, coverslips were incubated with primary antibodies (1:250 dilution) in PBS containing 2% BSA (16 h at 4 C), followed by 1 h of incubation with secondary Alexa546 Fluor anti-mouse goat antibody (1:500; Molecular Probes, Eugene, OR) or Alexa488 Fluor anti-rabbit goat antibody (1:500; Molecular Probes). Coverslips were mounted on glass slides with Vectashield (Vector Laboratories, Burlingame, CA). Images were acquired on a Leica DM IRE2 confocal microscope or on Leica fluorescence microscope DM RXA2 (Leica Microsystems, Heerbrugg, Switzerland), as appropriate.

Measurement of ROS. Intracellular ROS production was assessed through the evaluation of dihydroethidium oxidation using a Jasco FP6200 spectrofluorimeter (Jasco, Easton, MD) (7). Cells were incubated with 20 mM dihydroethidium for 0.5 h at 37°C in a serum-free medium in the dark, then washed with PBS, collected, and resuspended in assay buffer (100 mM potassium phosphate pH 7.4 and 2 mM $MgCl_2$), using an aliquot for protein determination. The fluorescence increase (480-nm excitation and 567-nm emission wavelengths) caused by the ROS-dependent oxidation of dihydroethidium was expressed as arbitrary units normalized by cell protein content.

Gene expression analysis. RNA was extracted using RNeasy mini-kit (Qiagen, Hilden, Germany), according to the manufacturer's instructions, as described previously (18). After total RNA was isolated from HepG2 cells, genomic DNA contamination was eliminated by DNase digestion (Qiagen), and cDNA was obtained using the High Capacity cDNA Reverse Transcription Kit (Applied Biosystems, Weiterstadt, Germany). Oligonucleotide primers used for quantitative (q)RT-PCR was as follows: human β-glucoronidase: forward CTCATTTGGAATTTTGCCGATT, reverse CCGAGTGAAGATCC; human rRNA 18s: forward CGAACGTCTGCCCTATCAACTT, reverse ACCCGTGGTCACCATGGTA; human *Nrf2*: forward AAACCAGTGGATCTGCCAAC, reverse GACCGGGAATATCAGGAACA; human *CYP1A1*: forward GCTGACTTCATCCCTATTCTTCG, reverse TTTTGTAGTGCTCCTTGACCATCT; human *GSTA5*: forward CATTCACCTGGTGGAACTTTTCTA, reverse CTGCCAGGCTGCAGAAACTT; human *GSTM2*: forward CCGATTTGAGGGCTTGGA, reverse CCATCTTTGTGAACACAGGTCTTG; human *SOD2*: forward GTTGGCTTGGTTTCAATAAGGAA, reverse TCCCCAGCAGTGGAATAAGG; and human catalase: forward TTCGATCTCACCAAGGTTTGG, reverse TGGATTCCGGTTTAAGACCAGTT.

The PCR reactions were carried out in an ABI PRISM 7500 System (Applied Biosystems, Weiterstadt, Germany). The PCR reactions were carried out under the following conditions: 50°C for 2 min, 95°C for 10 min, 40 cycles at 95°C for 15 s, and 60°C for 1 min. Relative gene expression levels were determined by analyzing the changes in SYBR green fluorescence during qRT-PCR using the ΔΔCt method. To confirm amplification of specific transcripts, melting curve profiles were produced at the end of each reaction. The mRNA level of each gene was normalized using β-actin as internal control.

Assessment of oxidative DNA damage. Oxidative DNA damage in the HepG2 cells was estimated by measuring the levels of 8-oxo-7,8-dihydro-2′-deoxyguanosine (8-oxodG) in DNA using the method of Polytarchou et al. (26). Briefly, HepG2 cells were fixed in 4% formaldehyde, either before or 30 min after treatment with H_2O_2, and then stained with an anti-8-hydroxyguanine antibody. Coverslips were mounted on glass slides, with Vectashield mounting medium containing 4′,6-diamidino-2-phenylindole (DAPI; Vector Laboratories). Images were obtained using a Nikon Eclipse 80i microscope with a ×10 objective and a Spot charge-coupled-device camera. Images were quantified as red/blue ratios by using Adobe Photoshop (Adobe Systems).

Ex vivo studies in liver biopsies. Liver biopsy specimens were obtained from patients admitted to the Liver Unit (Clinical Division "A. Murri," Azienda Ospedaliero-Universitaria Policlinico) with clinical and analytic features of ASH, including alcohol intake >80 g/day, increased aminotransferase and γ-glutamyl transpeptidase levels, and no other identifiable cause of liver disease (9). Histologic grading was as follows: *1*) degree of hepatocellular damage/ballooning (0, none; 1, mild; 2, severe) and presence of Mallory bodies, mega-mitochondria, and cholestasis (0, no; 1, yes); *2*) degree of lymphocytic infiltration (0, none; 1, mild; 2, moderate; 3, severe); *3*) degree of polymorphonu-

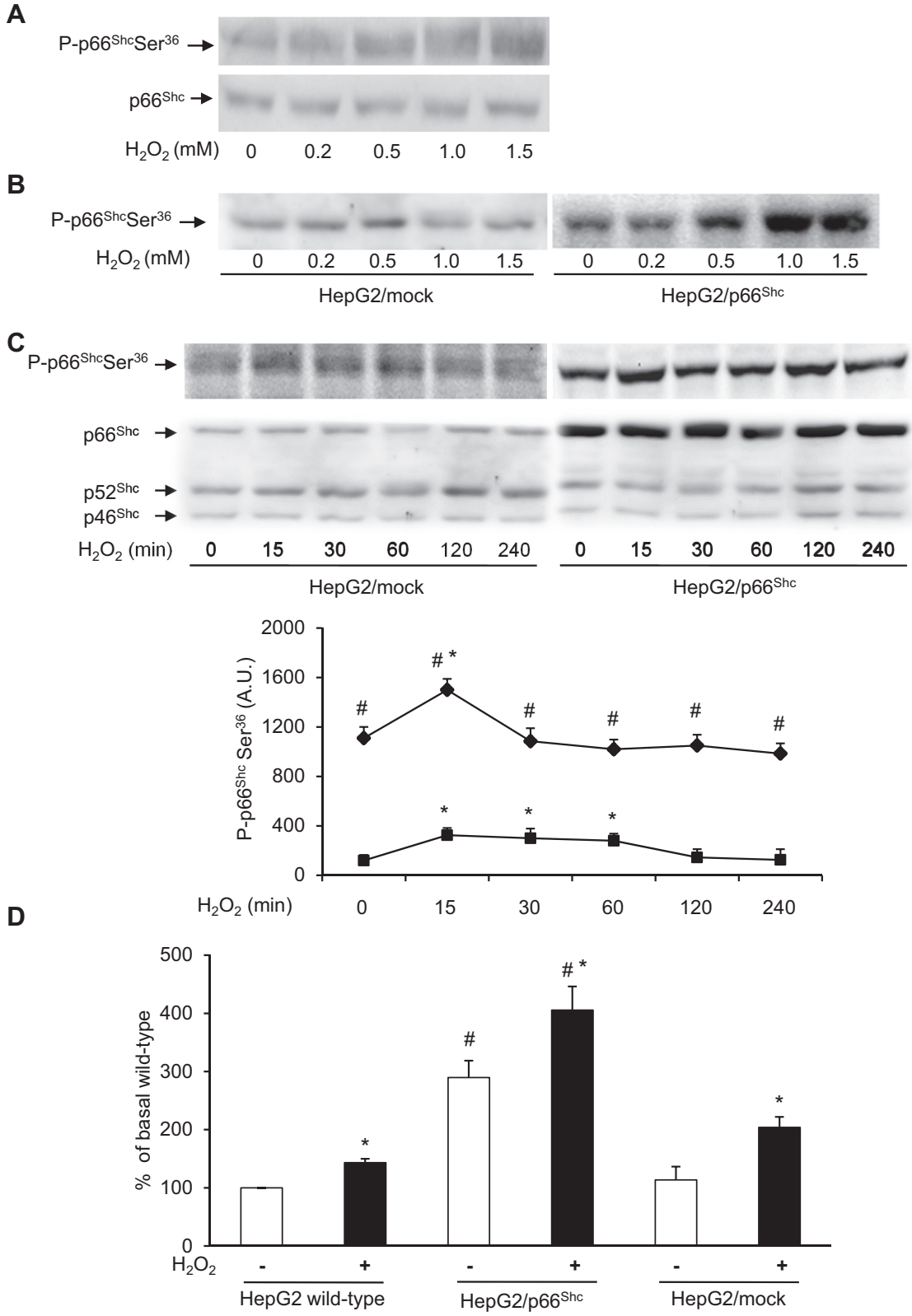

Fig. 1. p66Shc phosphorylation on Ser36 and reactive oxygen species (ROS) synthesis in HepG2 cells. *A*: dose-response of p66Shc phosphorylation on Ser36 in wild-type HepG2 cells exposed to H_2O_2 for 15 min. Representative immunoblots of p66Shc phosphorylation (*top*) and protein content (*bottom*) are shown. *B*: dose response of p66Shc phosphorylation on Ser36 in HepG2/p66Shc and HepG2/mock cells exposed to H_2O_2 for 15 min. *C*: time course of p66Shc phosphorylation in HepG2/p66Shc and HepG2/mock cells exposed to 0.5 mM H_2O_2. Representative immunoblots of p66Shc phosphorylation on Ser36 (*top*) and Shc protein content (*bottom*; all 3 Shc protein isoforms are shown). The quantitation of phosphorylated p66Shc on Ser36 in multiple experiments is also shown (◆: HepG2/p66Shc; ■: HepG2/mock). *D*: quantification of ROS levels in wild-type HepG2, HepG2/p66Shc, and HepG2/mock cells stimulated with H_2O_2 for 15 min (black bars) or left untreated (white bars). Results in *A–D* represent the means ± SE of at least $n = 5$ independent experiments. A.U., arbitrary units. *$P < 0.05$ vs. basal; #$P < 0.05$ vs. wild-type HepG2 and HepG2/mock.

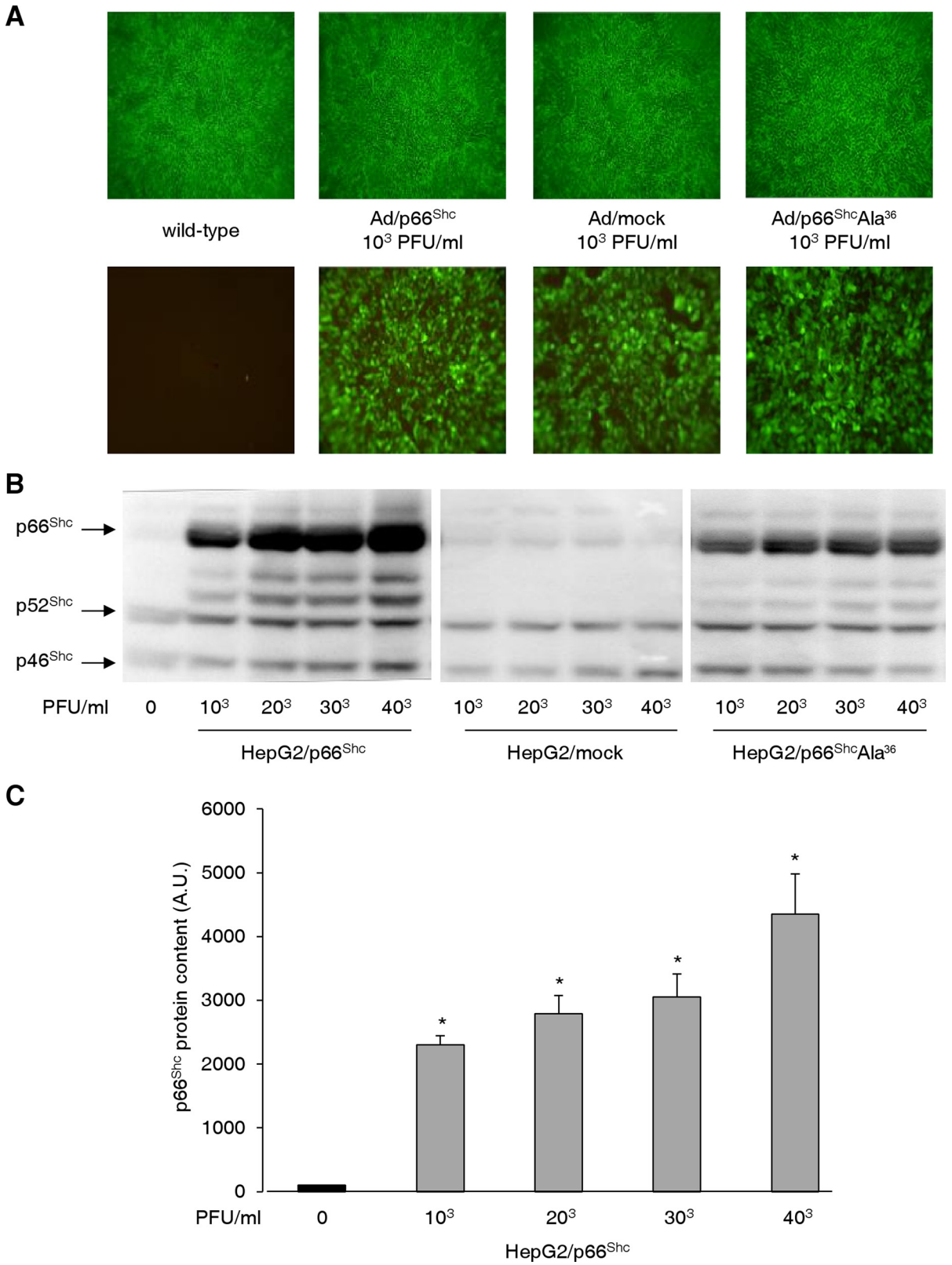

Fig. 2. p66Shc overexpression in HepG2 cells. HepG2 cells were transduced with different doses of Ad/p66Shc, Ad/mock, and Ad/p66ShcAla36 adenoviral constructs, expressing a green fluorescence protein, at 90% confluence, as described in MATERIALS AND METHODS. *A*: morphology of confluent wild-type HepG2, HepG2/p66Shc, HepG2/mock, and Ad/p66ShcAla36 cells incubated with the indicated doses of adenovirus under light microscopy (*top*) and corresponding fluorescent signal assessed under a fluorescent microscope (*bottom*). PFU, plaque-forming units. Magnification: ×10. *B*: representative immunoblot of all 3 Shc isoforms in HepG2/p66Shc, HepG2/mock, and Ad/p66ShcAla36 cells incubated with the indicated doses of adenovirus or left untreated. *C*: quantitation of p66Shc in HepG2/p66Shc incubated with the indicated doses of adenovirus or left untreated. *$P < 0.05$ vs. control.

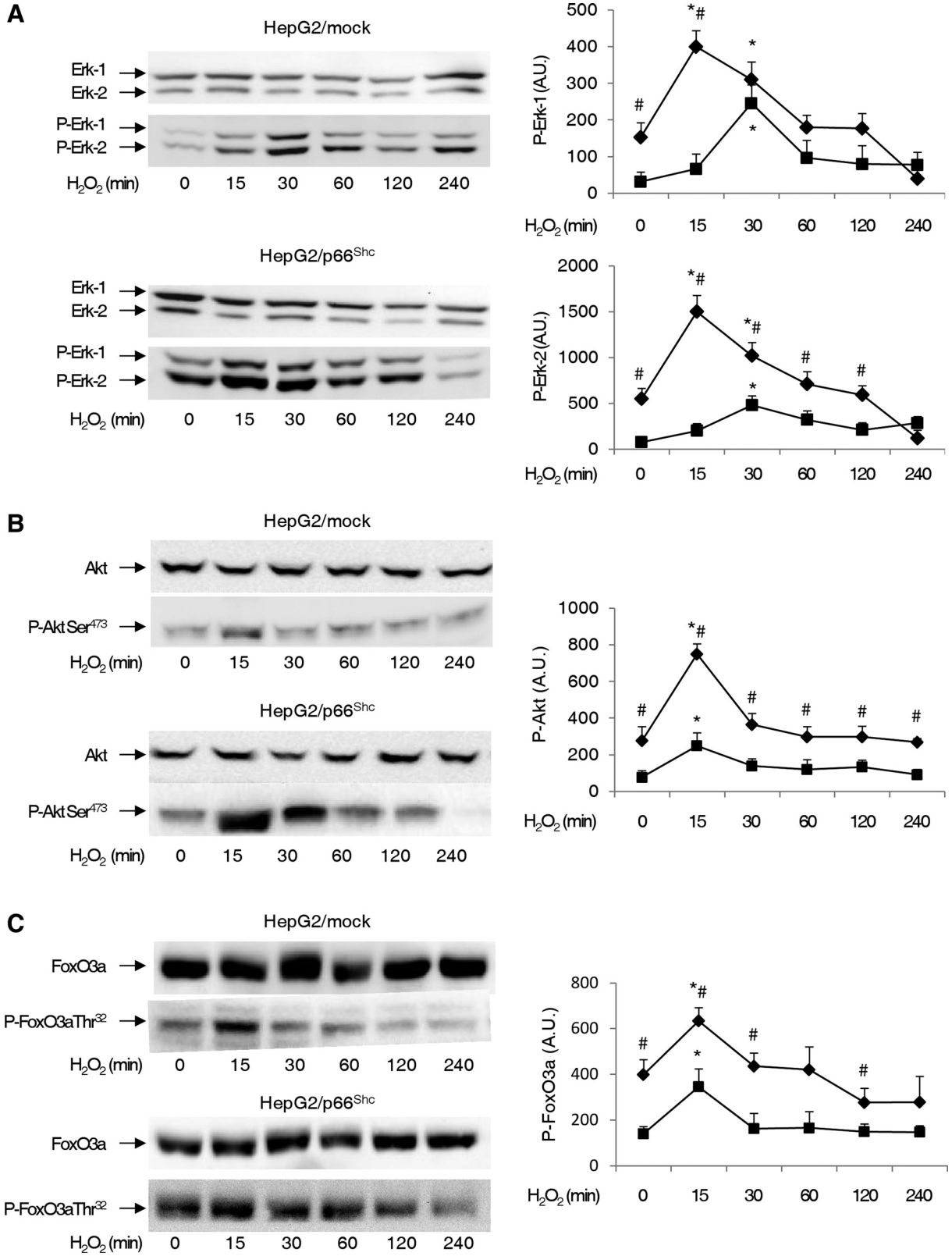

Fig. 3. Activation of Erk-1/2 and Akt/FoxO3a in HepG2/p66^{Shc} and HepG2/mock cells. HepG2/p66^{Shc} and HepG2/mock cells were incubated with 0.5 mM H_2O_2 for the indicated times or left untreated. Representative immunoblots of Erk-1/2 (*A*), Akt (*B*), and FoxO3a (*C*) total protein content and phosphorylation (*left*), and the quantitation of results from multiple experiments (*right*: ◆: HepG2/p66^{Shc}; ■: HepG2/mock). Results represent the mean ± SE of at least $n = 5$ independent experiments. *$P < 0.05$ vs. basal; #$P < 0.05$ vs. HepG2/mock.

clear infiltration (0, none; 1, mild; 2, moderate; 3, severe); *4*) degree of steatosis (G0: <10%; G1 10–33%; G2, 33–66%; G3 ≥66%); *5*) degree of lobular fibrosis (0, none; 1, mild; 2, moderate; 3, severe); and *6*) fibrosis stage (0, no fibrosis; 1, portal; 2, portal fibrosis and few septa; 3, septal fibrosis without cirrhosis; 4, cirrhosis) (9, 20). The protocol was approved by the Independent Ethics Committee at the Azienda Ospedaliero-Universitaria Policlinico Consorziale, Bari, Italy, and all patients gave their written informed consent.

Statistical analysis. Data are presented as means ± SE. Normal distribution of data was assessed by the Kolmogorov-Smirnov test ($P > 0.05$). Statistical analysis was performed by the Student's *t*-test or the one-way ANOVA with Tukey's multiple comparison test, as appropriate, using Minitab 15.1. Significance was assumed at $P < 0.05$.

RESULTS

p66Shc is activated by oxidative stress and promotes ROS synthesis in HepG2 cells. To understand the relationship between oxidative stress and p66Shc, p66shc phosphorylation was examined in HepG2 cells exposed to H_2O_2. Although the endogenous p66Shc levels were relatively low in wild-type HepG2 cells, phosphorylation of p66Shc on Ser36 could be detected in a dose-dependent manner upon exposure to H_2O_2 (Fig. 1*A*), and this was associated with increased intracellular ROS levels (Fig. 1*D*). To investigate the effects of increased p66Shc protein levels in liver cells, HepG2 cells with selective overexpression of p66Shc (HepG2/p66Shc) were obtained by infection with a recombinant adenovirus encoding p66Shc (Fig. 2). In the absence of H_2O_2, phosphorylation of p66Shc on Ser36 was found to be increased severalfold in HepG2/p66Shc compared with control HepG2/mock cells ($P < 0.0001$; Fig. 1, *B* and *C*), and it was further enhanced in a dose-dependent manner upon H_2O_2 exposure (Fig. 1B), peaking at 15 min ($P < 0.001$ vs. basal; Fig. 1*C*). ROS levels were increased approximately threefold in HepG2/p66Shc compared with control cells under basal conditions ($P < 0.001$ vs. wild-type HepG2 and HepG2/mock; Fig. 1*D*). In addition, exposure of HepG2/p66Shc cells to H_2O_2 led to further increase in ROS synthesis ($P < 0.005$ vs. wild-type HepG2 and HepG2/mock; Fig. 1*D*). Thus p66Shc conveys extracellular oxidative stress signals to increase ROS synthesis in liver cells.

p66Shc activates the Erk and Akt/FoxO3a pathways in HepG2 cells. The activation of Erk and of Akt/FoxO3a pathways, which have been shown to be involved in p66Shc signaling and oxidative stress responses (5, 11), was assessed next. Phosphorylation levels of Erk-1/2 (Fig. 3*A*) and Akt (Fig. 3*B*) were found to be significantly increased in response to

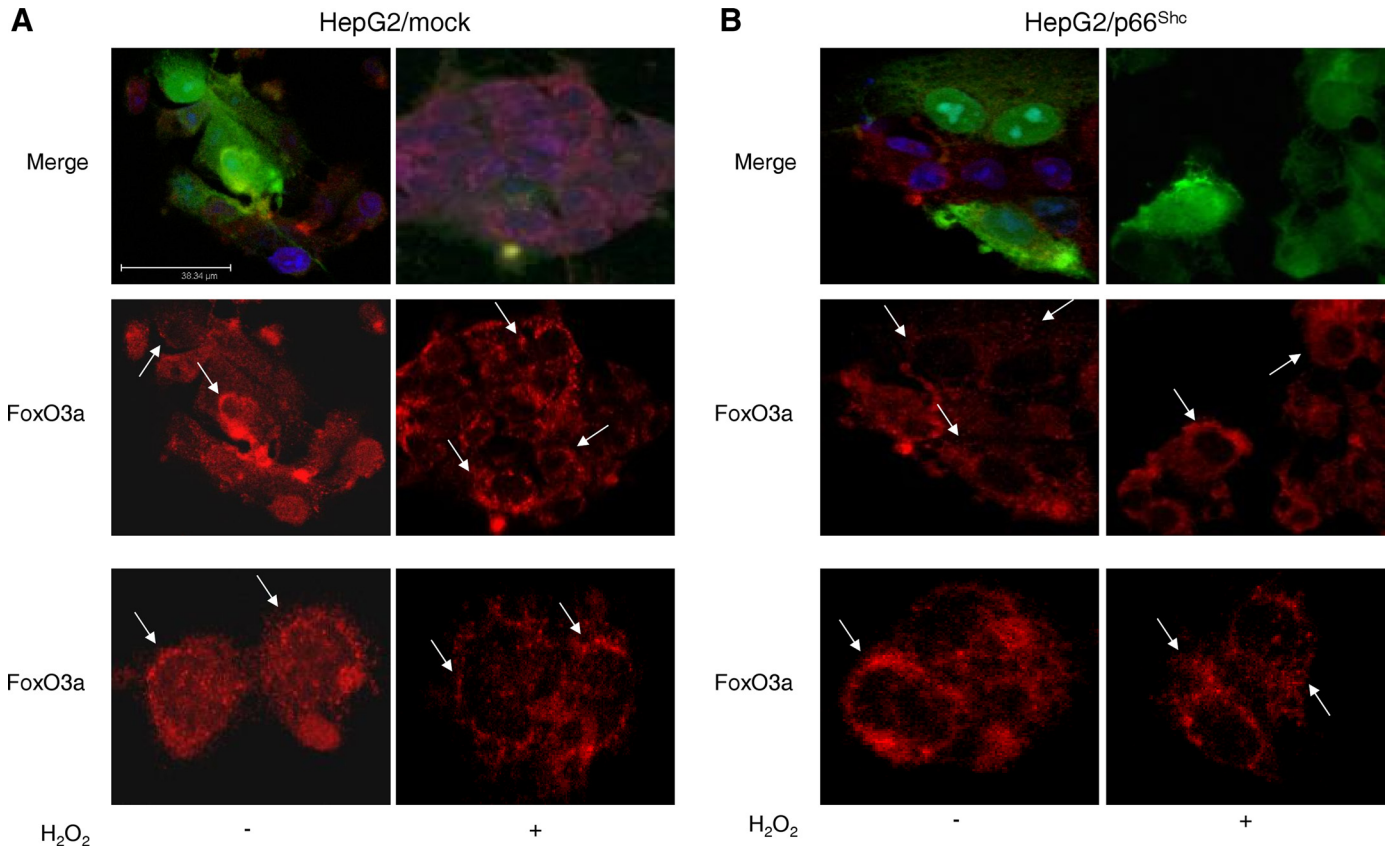

Fig. 4. FoxO3a localization in HepG2/mock and HepG2/p66Shc cells. HepG2/mock (*A*) and HepG2/p66Shc (*B*) cells were incubated with 0.5 mM H_2O_2 for 15 min or left untreated. The magnified images show FoxO3a localization in representative HepG2/mock and HepG2/p66Shc cells. Adenovirus-infected cells are shown in green according to green fluorescence protein expression (green, *top*). FoxO3a was visualized with a rabbit polyclonal antibody followed by the addition of ALEX488 (red) labeled anti-rabbit antisera. TOPRO (blue) was used to visualize the nuclei. In control HepG2/mock cells, endogenous FoxO3a could be detected almost exclusively in the cell nucleus in the absence of H_2O_2 (*A*, white arrows in images on the *left*), whereas it was relocated predominantly in the cytoplasm after exiting the nucleus following H_2O_2 stimulation for 15 min (*A*, white arrows in images on the *right*). In HepG2/p66Shc cells, FoxO3a showed predominant cytoplasmic localization and reduced nuclear staining already in the absence of H_2O_2 (*B*, white arrows in images on the *left*), and this was not significantly modified by exposure to H_2O_2 (*B*, white arrows in images on the *right*). Images are representative of 4 independent experiments.

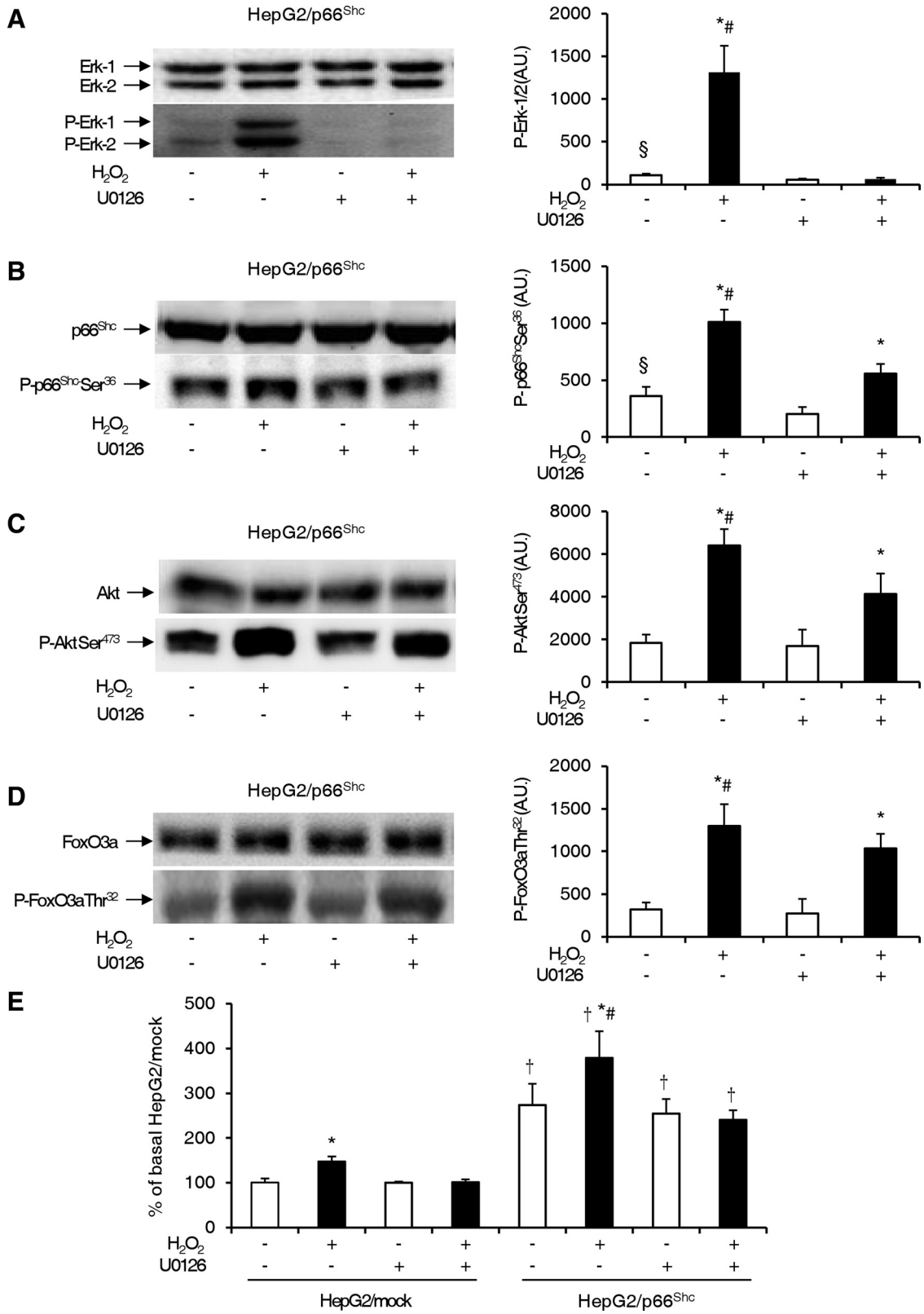

Fig. 5. Effects of the MEK inhibitor on p66^{Shc} phosphorylation, Akt/FoxO3a signaling, and ROS production. Representative immunoblots (*left*) assessing total protein content and phosphorylation of Erk-1/2 (*A*), p66^{Shc} (*B*), Akt (*C*), and FoxO3a (*D*) in HepG2/p66^{Shc} cells. The quantitation of results from multiple experiments is also shown (*right*). HepG2/p66^{Shc} were pretreated with 20 μM U0126 for 2 h or left untreated before exposure to 0.5 mM H_2O_2 for 15 min. *E*: quantitation of ROS levels in HepG2/mock and HepG2/p66^{Shc} cells stimulated with 0.5 mM H_2O_2 for 15 min (black bars) or left untreated (white bars). Results represent the means ± SE of at least $n = 5$ independent experiments. *$P < 0.05$ vs. basal; #$P < 0.05$ vs. H_2O_2-stimulated cells treated with U0126; §$P < 0.05$ vs. unstimulated HepG2/mock treated with U0126; †$P < 0.05$ vs. HepG2/mock.

H_2O_2 treatment in both HepG2/p66^{Shc} and HepG2/mock cells ($P < 0.001$ vs. basal; Fig. 3, *A* and *B*). However, Erk-1/2 and Akt phosphorylation showed higher levels and Erk-1/2 also an earlier 15-min peak after H_2O_2 challenge in HepG2/p66^{Shc} than in control cells ($P < 0.001$ vs. HepG2/mock; Fig. 3, *A* and *B*). Both JNK-1/2 and p38 MAPK were also found to be activated upon H_2O_2 treatment in both HepG2/p66^{Shc} and control cells; however, phosphorylation levels of these kinases were similar in HepG2/p66^{Shc} and control cells (data not shown).

Akt-mediated FoxO3a phosphorylation on Thr^{32} promotes both its inactivation and translocation from the nucleus to the cytoplasm (8). In both HepG2/mock and HepG2/p66^{Shc} cells, the levels of Thr^{32} phosphorylation of FoxO3a were increased following challenge with H_2O_2 ($P < 0.005$ vs. basal; Fig. 3*C*) and augmented in p66^{Shc} overexpressing vs. control cells ($P < 0.005$ in HepG2/p66^{Shc} vs. HepG2/mock; Fig. 3*C*), paralleling Akt phosphorylation (Fig. 3*B*). The subcellular distribution of FoxO3a in the cytoplasmic and nuclear compartment was then investigated. In control HepG2/mock cells, endogenous FoxO3a could be detected almost exclusively in the nucleus in the basal state, whereas it was relocated predominantly in the cytoplasm following 15 min of H_2O_2 stimulation (Fig. 4*A*). By contrast, in HepG2/p66^{Shc} cells, FoxO3a showed reduced nuclear staining and increased cytoplasmic localization already in the basal state, with minimal changes induced by exposure to H_2O_2 (Fig. 4*B*). Thus H_2O_2-mediated p66^{Shc} activation is followed by activation of the Erk-1/2 and Akt/FoxO3a pathways and translocation of FoxO3a from the nuclear to the cytoplasmic compartment. These responses are enhanced, and already under basal conditions, when p66^{Shc} is overexpressed.

Role of ERK in Ser^{36} phosphorylation of p66^{Shc} and Akt/FoxO3a phosphorylation. The role of Erk-1/2 activation in p66^{Shc} phosphorylation was investigated next by using the MEK inhibitor U0126. As expected, pretreatment with U0126 completely abrogated Erk-1/2 phosphorylation in both HepG2/mock and HepG2/p66^{Shc} cells, both under basal conditions and after H_2O_2 stimulation ($P < 0.0001$ vs. cells not exposed to U0126; Fig. 5*A* and data not shown). This was associated with a significant decrease in p66^{Shc} phosphorylation on Ser^{36}, both in the absence and presence of H_2O_2 (Fig. 5*B* and data not shown). Similar results were obtained using PD098059, another inhibitor of MEK (data not shown). Furthermore, inhibiting the Erk-1/2 pathway with U0126 also significantly reduced the phosphorylation of Akt and FoxO3a following H_2O_2 challenge ($P < 0.05$ vs. cells not exposed to the MEK inhibitor; Fig. 5, *C* and *D*). Finally, treatment with U0126 markedly reduced H_2O_2-induced ROS production in control and HepG2/p66^{Shc} cells, respectively ($P < 0.01$ vs. cells not exposed to U0126; Fig. 5*E*). Altogether, these results suggest that activation of Erk-1/2 contributes to p66^{Shc} phosphorylation and its downstream signaling.

Role of p66^{Shc} Ser^{36} phosphorylation in Erk and Akt/FoxO3a signaling and ROS production. To assess whether phosphorylation of p66^{Shc} on Ser^{36} is necessary for efficient signal propagation, a phosphorylation-defective p66^{Shc} protein, in which Ser^{36} was mutated to Ala, was overexpressed in HepG2 cells (HepG2/p66^{Shc}-Ala^{36}). No significant differences in p66^{Shc} protein levels were observed between HepG2/p66^{Shc} and HepG2/p66^{Shc}-Ala^{36} cells (Fig. 6*A*), while Ser^{36} phosphorylation of p66^{Shc} was undetectable in HepG2/p66^{Shc}-Ala^{36} cells both under basal conditions and after H_2O_2 stimulation

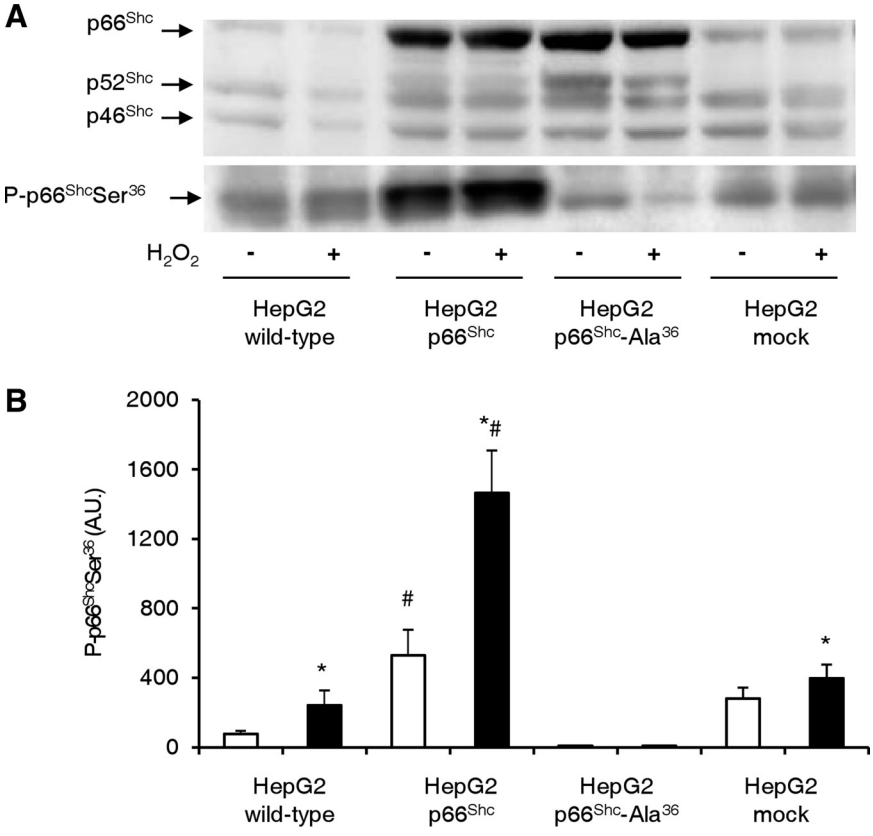

Fig. 6. p66^{Shc} phosphorylation on Ser^{36} in HepG2 cells overexpressing the mutant p66^{Shc}Ala^{36} protein. *A*: representative immunoblots of Shc protein content (*top*) and p66^{Shc} phosphorylation on Ser^{36} (*bottom*). *B*: densitometric analysis of 5 independent experiments (white bars: untreated cells; black bars: H_2O_2-stimulated cells). Wild-type HepG2, HepG2/p66^{Shc}, HepG2/p66^{Shc}-Ala^{36}, and HepG2/mock cells were incubated with 0.5 mM H_2O_2 for 15 min or left untreated. Data represent the quantitation of at least $n = 5$ independent experiments. *$P < 0.05$ vs. basal; #$P < 0.05$ vs. wild-type HepG2, HepG2/mock, and HepG2/p66^{Shc}-Ala^{36}.

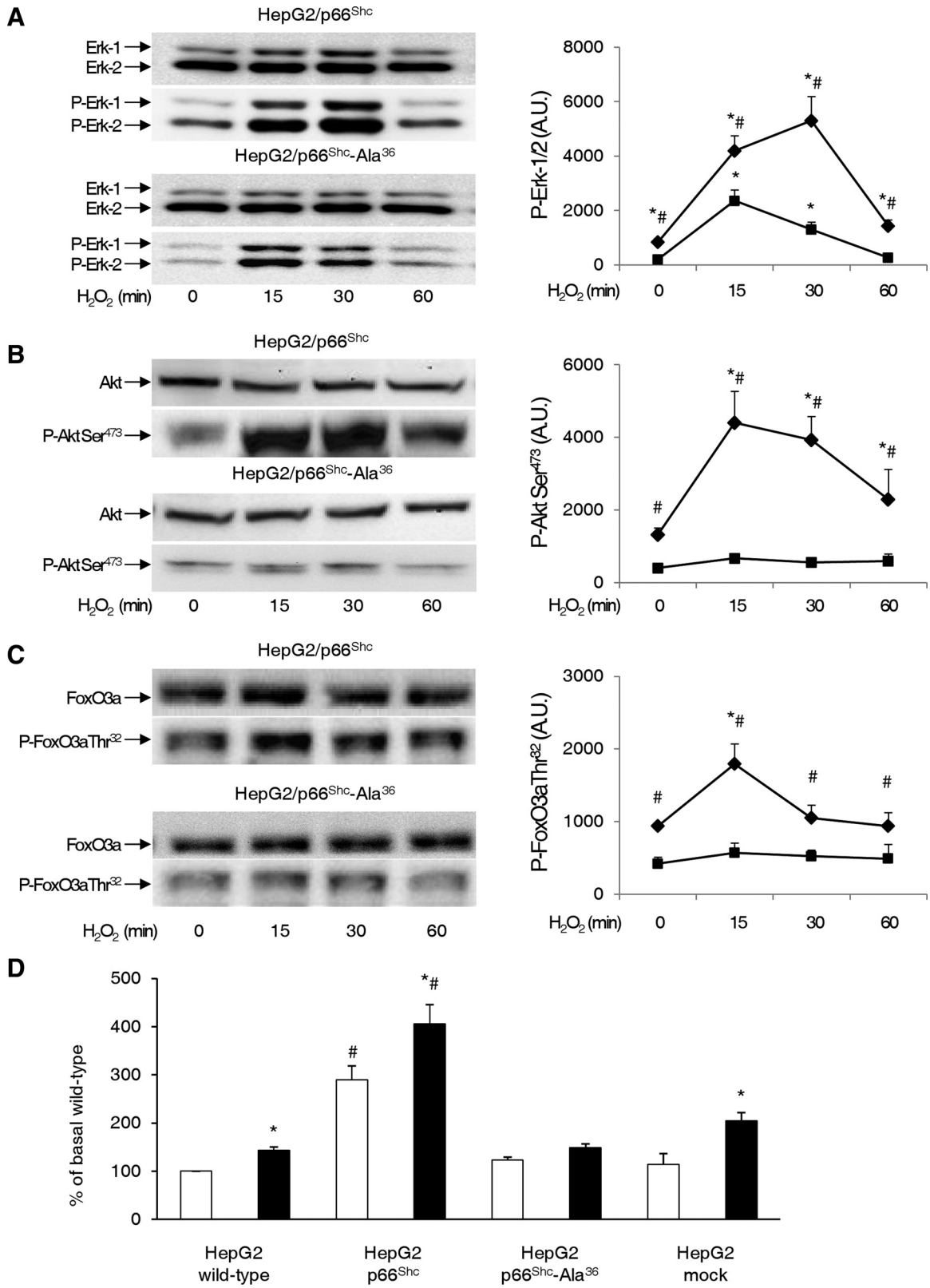

Fig. 7. Activation of Erk and Akt/FoxO3a pathways and ROS synthesis in HepG2 cells overexpressing the phosphorylation defective p66^{Shc} Ala^{36} mutant. HepG2/p66^{Shc} and HepG2/p66^{Shc}-Ala^{36} cells were incubated with 0.5 mM H_2O_2 for the indicated times or left untreated. Representative immunoblots (*left*) of Erk-1/2 (*A*), Akt (*B*), and FoxO3a (*C*) total protein content and phosphorylation, respectively. The quantitation of results from multiple experiments is also shown (*right*: ◆: HepG2/p66^{Shc}; ■: HepG2/p66^{Shc}-Ala^{36}). Results represent the means ± SE of at least $n = 5$ independent experiments. *$P < 0.05$ vs. basal; #$P < 0.05$ vs. HepG2/p66^{Shc}-Ala^{36}. *D*: quantification of ROS levels in wild-type HepG2, HepG2/p66^{Shc}, HepG2/p66^{Shc}-Ala^{36}, and HepG2/mock cells stimulated with 0.5 mM H_2O_2 for 15 min (black bars) or left untreated (white bars). Data represent the quantitation of at least $n = 5$ independent experiments. *$P < 0.05$ vs. basal; #$P < 0.05$ vs. wild-type HepG2, HepG2/mock, and HepG2/p66^{Shc}-Ala^{36}.

(Fig. 6, *A* and *B*). Interestingly, Erk-1/2 activation was significantly decreased and Akt/FoxO3a phosphorylation was completely blunted in HepG2/p66^{Shc}-Ala^{36} compared with HepG2/p66^{Shc} cells, both in the absence and presence of H_2O_2 stimulation (Fig. 7, *A–C*; $P < 0.01$ vs. HepG2/p66^{Shc}). In addition, H_2O_2 exposure failed to increase ROS production in HepG2/p66^{Shc}-Ala^{36}, differently than in control cells (Fig. 7*D*), indicating that Ser^{36} phosphorylation of p66^{Shc} is critical for ROS production in response to oxidative stress. Thus Ser^{36} phosphorylation of p66^{Shc} plays an important role in activation of the Erk and Akt/FoxO3a signaling pathways and ROS synthesis in HepG2 cells.

Nrf2 and Nrf2 target genes in HepG2 cells overexpressing p66^{Shc}. In the light of the protective role of *Nrf2* against oxidative stress (17–19), whether *Nrf2* and the Nrf2-induced antioxidant response element (ARE) target genes would be affected by changes in p66^{Shc} protein levels in HepG2 cells was examined next. Interestingly, *Nrf2* mRNA levels were significantly lower in HepG2/p66^{Shc} than in control HepG2/mock cells in the absence of H_2O_2 ($P < 0.05$ vs. basal control cells; Fig. 8) and remained significantly reduced by >50% at multiple times following induction of oxidative stress with H_2O_2 up to 240 min ($P < 0.05$ vs. control cells at 15–60 min; Fig. 8). Changes in *Nrf2* mRNA levels were paralleled by

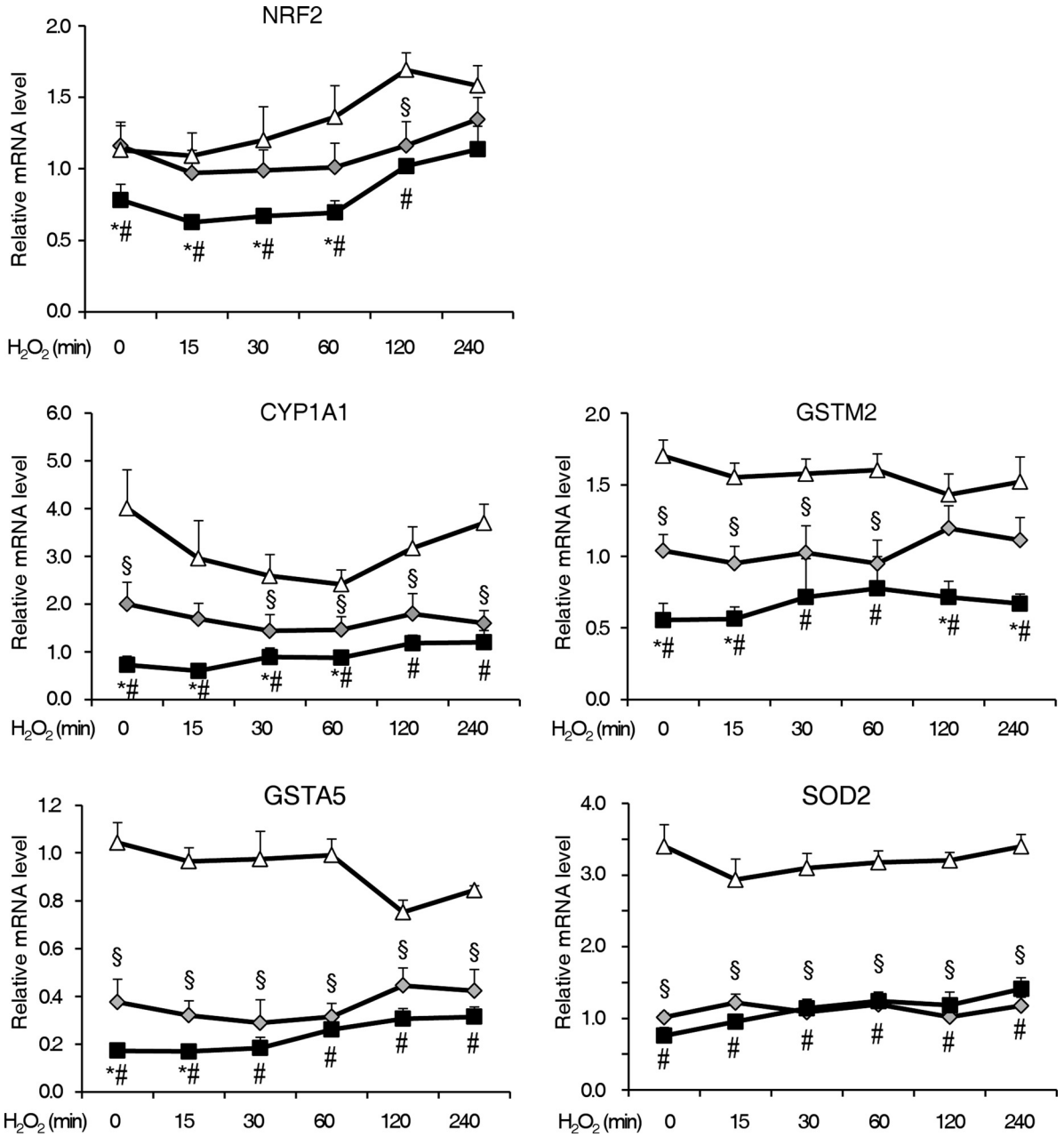

Fig. 8. mRNA expression levels of NF-E2-related factor 2 (*Nrf2*) and Nrf2-target genes in HepG2/mock, HepG2/p66^{Shc}, and HepG2/p66^{Shc}-Ala^{36} cells. *Nrf2*, *CYP1A1*, *GSTM2*, *GSTA5*, and *SOD2* mRNA expression levels were measured by quantitative RT-PCR in HepG2/mock (grey squares), HepG2/p66^{Shc} (black squares), and HepG2/p66^{Shc}-Ala^{36} (white triangles) following exposure to 0.5 mM H_2O_2 for the indicated times. Data represent the means ± SE of at least $n = 5$ independent experiments. *$P < 0.05$ HepG2/p66^{Shc} vs. HepG2/mock; #$P < 0.05$ HepG2/p66^{Shc} vs. HepG2/p66^{Shc}-Ala^{36}; §$P < 0.05$ HepG2/p66^{Shc}-Ala^{36} vs. HepG2/mock.

similar changes in gene expression of major Nrf2 target genes. Indeed, mRNA levels of cytochrome P450 (*CYP*)*1A1*, *GSTM2*, and *GSTA5* were significantly reduced in HepG2/p66^{Shc} compared with HepG2/mock cells both under basal conditions and at multiple time-points following exposure to H_2O_2 ($P < 0.05$ vs. HepG2/mock; Fig. 8). Furthermore, *Nrf2* and Nrf2-induced ARE genes showed markedly reduced mRNA levels in HepG2/p66^{Shc} compared with HepG2/p66^{Shc}-Ala^{36} cells ($P < 0.05$ vs. HepG2/p66^{Shc}-Ala^{36}; Fig. 8). Finally, HepG2/p66^{Shc}-Ala^{36} cells exhibited higher mRNA levels of *CYP1A1*, *GSTM2*,

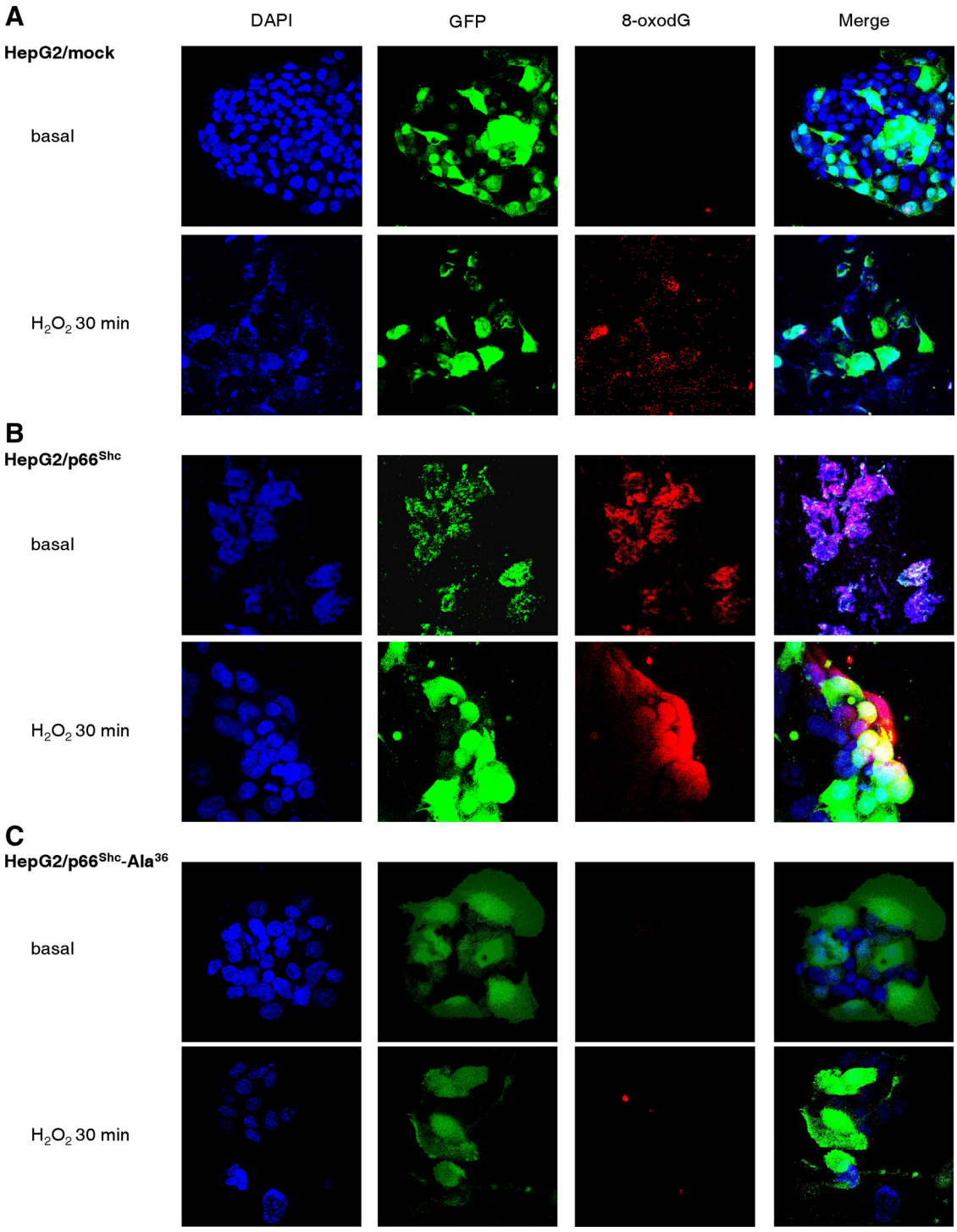

Fig. 9. 8-oxo-7,8-dihydro-2′-deoxyguanosine (8-oxodG) accumulation following p66^{Shc} overexpression in HepG2 cells. HepG2/mock (*A*), HepG2/p66^{Shc} (*B*), and HepG2/p66^{Shc}-Ala^{36} (*C*) cells were treated with 0.5 mM H_2O_2 or left untreated and then analyzed 30 min later by immunofluorescence, evaluating accumulation of 8-oxodG, a sensitive marker of DNA damage. For each condition, from *left* to *right*, the *1st column* shows DAPI nuclei staining, the *2nd column* shows the green fluorescence protein (GFP) in infected cells, the *3rd column* shows 8-oxodG staining, and the *4th column* displays the merged staining (*A*–*C*). Bar = 50 μm. Results are representative of $n = 4$ independent experiments.

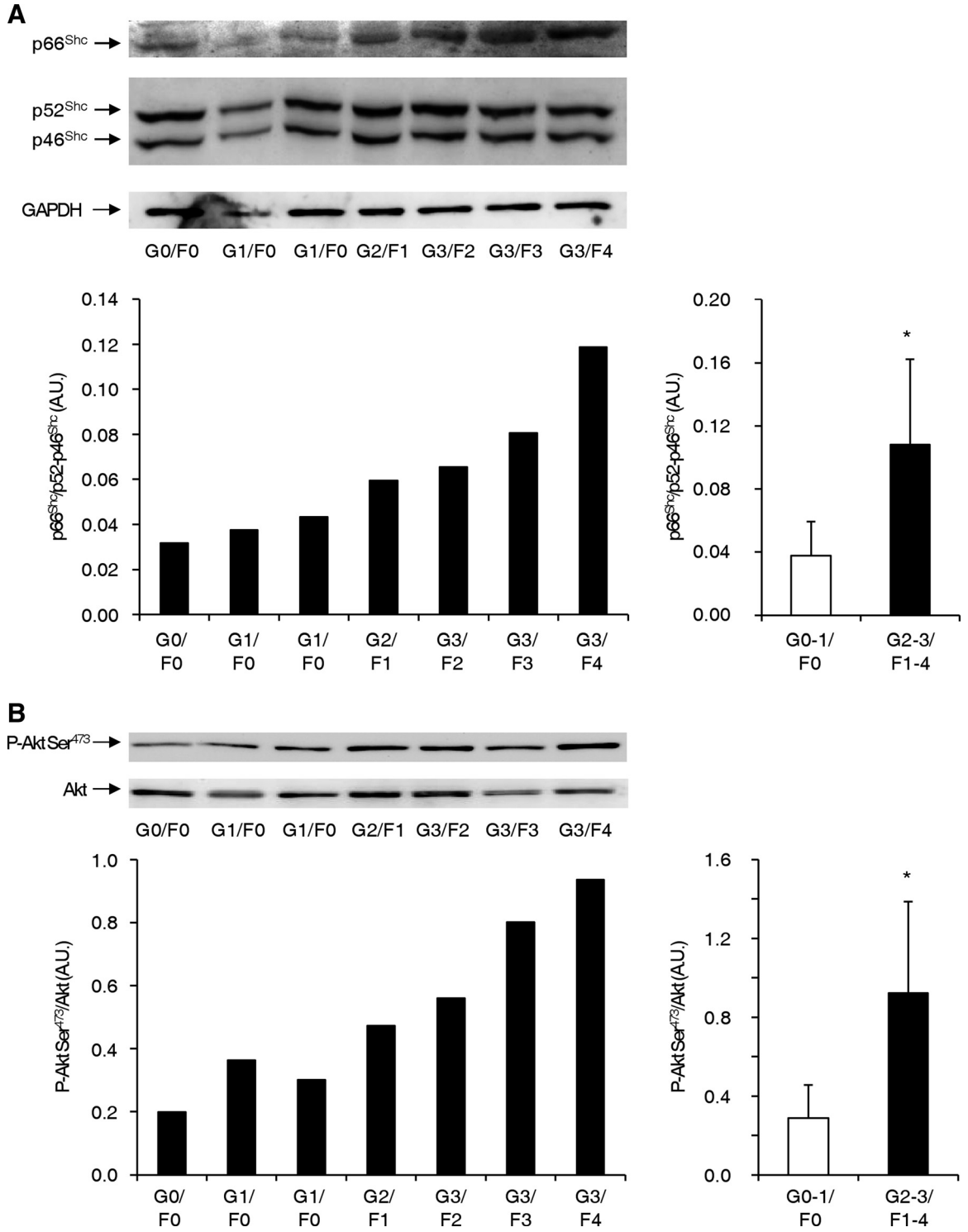

Fig. 10. Protein levels of p66Shc in liver from ASH subjects. *A*: protein levels of Shc isoforms in human liver biopsies. Representative immunoblots of Shc protein isoforms in liver biopsies from individual subjects with various degrees of steatosis, fibrosis, and lymphocytic/polymorphonuclear infiltration are shown (*top*). GAPDH protein content was used as loading control. The quantitation of p66Shc vs. p52-p46Shc ratio in liver samples considered individually (*bottom left*) and grouped as G0-1/F0 (steatosis <33% and absence of fibrosis and lymphocytic/polymorphonuclear infiltration) and as G2-3/F1-4 (steatosis >33% and presence of fibrosis and lymphocytic/polymorphonuclear infiltration; *bottom right*) is also shown. *B*: Akt in human liver biopsies. Representative immunoblots of Akt phosphorylation and total protein content in liver biopsies from individual subjects with various degrees of steatosis, fibrosis and lymphocytic/polymorphonuclear infiltration are shown (*top*). The quantitation of phospho-Akt vs. total Akt liver biopsies considered individually (*bottom left*) and grouped as G0-1/F0 and G2-3/F1-4 (*bottom right*) is also shown. $*P < 0.05$ vs. G0-1/F0.

GSTA5, and *SOD2* than control HepG2/mock cells ($P < 0.05$ vs. HepG2/mock; Fig. 8), consistent with the mutant $p66^{Shc}$ Ala^{36} variant acting as a dominant-negative protein.

Overexpression of $p66^{Shc}$ promotes oxidative DNA damage. 8-OxodG is a sensitive marker of ROS-induced DNA damage (27). To investigate the possibility that forced expression/activation of $p66^{Shc}$ may lead to DNA damage via increased ROS synthesis, the extent of 8-oxodG accumulation was assessed in individual cells infected with the distinct adenoviral constructs by immunofluorescence. Expression of green fluorescent protein by the adenovirus allowed identification of infected cells. With this method, 8-oxodG staining was found to be increased in HepG2/$p66^{Shc}$ compared with HepG2/mock and HepG2/$p66^{Shc}$-Ala^{36} cells in the absence of H_2O_2 (Fig. 9, *A–C*). Treatment of HepG2/$p66^{Shc}$ with H_2O_2 for 60 min further increased 8-oxodG accumulation at 15 min (data not shown) and 30 min (Fig. 9*B*). By contrast, 8-oxodG staining was almost undetectable in H_2O_2-treated HepG2/$p66^{Shc}$-Ala^{36} compared with both HepG2/$p66^{Shc}$ and HepG2/mock cells (Fig. 9, *A–C*). Overall, these data demonstrate that $p66^{Shc}$ promotes ROS-induced DNA damage in liver cells and that this is inhibited by the phosphorylation-defective $p66^{Shc}$ protein.

$p66^{Shc}$ in human liver biopsies from subjects with ASH. Finally, protein expression and phosphorylation levels of $p66^{Shc}$ were examined in liver biopsies of subjects with ASH. The severity of liver injury was graded according to the presence and extent of steatosis, fibrosis, and lymphocytic/polymorphonuclear infiltration (9, 20), ranging from G0/F0 to G3/F4. The protein levels of $p66^{Shc}$ were found to be increased in the human liver biopsies in parallel with the severity of liver injury (Fig. 10*A*), in the absence of changes in $p52^{Shc}$ and $p46^{Shc}$ protein abundance (Fig. 10*A*). Furthermore, $p66^{Shc}$ expression was found to be significantly increased in the group with higher extent of steatosis (>33%) and presence of fibrosis and lymphocytic/polymorphonuclear infiltration ($P < 0.05$, G2-3/F1-4 vs. G0-1/F0; Fig. 10*A*). Furthermore, increased $p66^{Shc}$ protein levels were associated with significant augmentation of Akt phosphorylation, in the absence of significant changes in Akt protein levels ($P < 0.05$, G2-3/F1-4 vs. G0-1/F0; Fig. 10*B*). Other signaling reactions, including $p66^{Shc}$ phosphorylation on Ser^{36} and FoxO3a phosphorylation on Thr^{32}, could not be assessed since they were below the sensitivity of the immunoblotting technique (data not shown).

DISCUSSION

The adapter protein $p66^{Shc}$ has been shown to mediate oxidative stress-related injury in multiple cell types and under a variety of pathophysiological conditions, including obesity, diabetes, and steatohepatitis (1, 10–13, 19, 21, 24, 25, 27–32, 36). Specifically, $p66^{Shc}$ has been involved in hepatocyte lipid accumulation and cytotoxicity in both experimental ethanol intoxication and NASH (17, 31). The results from this study demonstrate for the first time that $p66^{Shc}$ is both a target and an enhancer of oxidative stress in liver cells and that $p66^{Shc}$ protein levels are increased in the liver of individuals with ASH. In addition, forced expression of $p66^{Shc}$ promotes ROS synthesis and reduces expression of Nrf2 and Nrf2-induced ARE genes, increasing incorporation of 8-oxodG into cellular DNA, a marker of oxidative stress-related DNA damage. All of these effects require phosphorylation of $p66^{Shc}$ on Ser^{36}.

In control HepG2 cells the levels of $p66^{Shc}$ were relatively low, yet phosphorylation of the protein could be induced by exposure to H_2O_2. However, when $p66^{Shc}$ was overexpressed by adenoviral-mediated gene transfer its phosphorylation on Ser^{36} was increased (Fig. 1*C*) and this was associated with increased phosphorylation of Erk-1/2 and Akt/FoxO3a (Fig. 3, *A–C*) and ROS synthesis (Fig. 1*D*).

While overexpression of $p66^{Shc}$ was associated with increased Erk-1/2 phosphorylation, which was reduced in HepG2 overexpressing a defective $p66^{Shc}$-Ala^{36} (Fig. 7*A*), inhibition of the Erk pathway using various MEK inhibitors significantly reduced Ser^{36} phosphorylation of $p66^{Shc}$ both in the absence and presence of H_2O_2 stimulation. Altogether, these results suggest that $p66^{Shc}$ and Erk-1/2 are involved in a reciprocal "regulatory loop": increased $p66^{Shc}$ expression/signaling results in Erk-1/2 activation that in turn promotes Ser^{36}-phosphorylation of $p66^{Shc}$ (Fig. 11). These data are in line with previous observations in breast and prostate cancer cells, in which increased $p66^{Shc}$ protein levels were positively correlated with Erk-1/2 phosphorylation (16, 34), and $p66^{Shc}$ knockdown led to reduced Erk-1/2 activation (34), but not with other studies showing inhibition of Erk signaling by $p66^{Shc}$ (32). Conversely, Erk-dependent phosphorylation of $p66^{Shc}$ on Ser^{36}, which is then responsible for $p66^{Shc}$-dependent phosphorylation of FoxO3a, as observed in this study (Fig. 5), was previously shown in mouse embryo fibroblasts (32). However, the phosphorylation levels of $p66^{Shc}$ on Ser^{36} were not completely abolished when Erk-1/2 was fully inhibited (Fig. 5), suggesting that additional protein kinases other than Erk-1/2 may be involved in Ser^{36}-phosphorylation of $p66^{Shc}$. Indeed, depending on the cell type and stimulus (e.g., H_2O_2, TGF-β, various cytokines), protein kinase C (PKC)-β and -δ and β1Pix (Pak-interacting exchange factor) have also been shown to be involved in $p66^{Shc}$ phosphorylation on Ser^{36} (6, 22, 31). Furthermore, we have recently reported that TNF-α promotes $p66^{Shc}$ phosphorylation on Ser^{36} via the stress-kinase JNK in human endothelial cells (23). However, both JNK-1/2 and p38

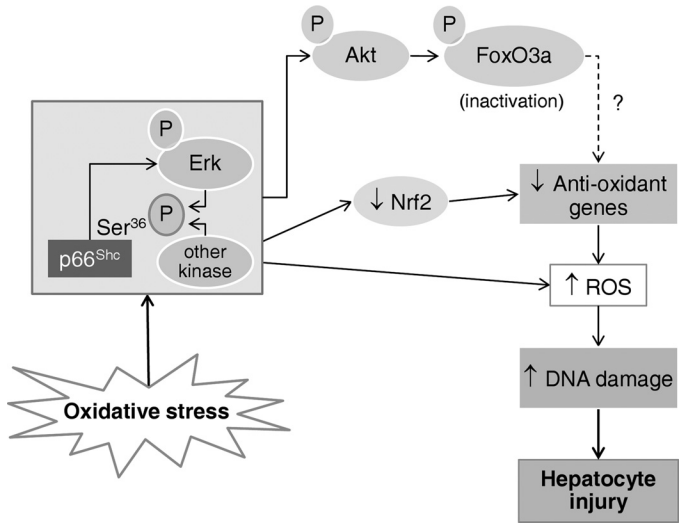

Fig. 11. Hypothetical model of $p66^{Shc}$-dependent redox signaling in human liver cells. P, phosphorylation.

MAPK activities were not affected by p66Shc overexpression in HepG2 cells (data not shown), suggesting that they are not part of the same regulatory loop as Erk-1/2.

The involvement of the *Nrf2* signaling pathway in eliciting cell survival and resistance to oxidative stress has been recently reported (2, 5, 35). *Nrf2* plays a central role in cytoprotection, by detoxifying and eliminating ROS, xenobiotics and electrophilic carcinogens, as well as by removing damaged proteins and organelles (35). Compared with control cells, *Nrf2* knockout cardiomyocytes showed significantly higher ROS levels under basal conditions, which were further enhanced upon exposure to high glucose concentrations (14). Similarly, in primary mouse hepatocytes *Nrf2* gene ablation resulted in enhanced oxidative stress, impaired activation of the MAPK pathway, and reduced mRNA expression of ROS-detoxifying enzymes (4). In line with these findings, our results show for the first time a link between the redox protein p66Shc and the *Nrf2* pathway. Liver cells overexpressing p66Shc showed reduced mRNA levels of *Nrf2* and of its downstream detoxifying target genes, such as *CYP1A1*, *GSTM2*, and *GSTA5*, in association with enhanced ROS synthesis and increased oxidative DNA damage. Conversely, cells overexpressing the phosphorylation-defective p66Shc mutant displayed augmentation of gene expression of *Nrf2* and its downstream target genes, reduced ROS levels, and minimal 8-oxodG accumulation. Thus, p66Shc appears to foster cellular oxidative stress responses by suppressing *Nrf2* expression (Fig. 11). The Akt/FoxO3a signaling pathway is also involved in preventing accumulation of ROS and consequent cell damage by upregulating antioxidant enzymes (33). Since forced activation of p66Shc resulted in increased FoxO3a phosphorylation and nuclear exclusion (Figs. 3 and 4), and this was not observed following overexpression of p66ShcAla36 (Fig. 7), enhanced p66Shc signaling may potentially promote oxidative DNA damage by both repressing *Nrf2* and inactivating FoxO3a (Fig. 11).

Significant elevations of *p66Shc* mRNA and protein levels were recently reported in liver biopsies from individuals with nonalcoholic fatty liver disease (NAFLD) and NASH, compared with normal liver samples (31). In line with these findings, we found increased p66Shc protein levels in liver biopsies of subjects with ASH, a well-characterized condition of oxidative stress-induced cellular damage (10, 29). Moreover, p66Shc protein abundance correlated with the degree of histological abnormalities and disease severity, being increased to a greater extent in subjects with higher degree of fibrosis and steatosis (Fig. 10), in line with the results in NAFLD/NASH (14). Increased protein expression of p66Shc in liver biopsies with more severe grading was associated with augmented Akt phosphorylation, suggesting the functional relevance of these findings (Fig. 10). Inhibition of hepatic p66Shc signaling may thus represent an attractive strategy to counteract progression of hepatocyte damage in both alcoholic and nonalcoholic fatty liver disease.

In conclusion, overexpression of p66Shc in human hepatocytes promotes ROS accumulation and increases susceptibility to H_2O_2-induced oxidative stress, leading to reduced levels of cytoprotective genes and consequently increased DNA damage. Modulation of the redox homeostasis by limiting p66Shc expression and/or activity in human hepatocytes may open novel therapeutic approaches for oxidative stress-associated liver diseases.

ACKNOWLEDGMENTS

We thank Dr. Alessandro Peschechera for technical assistance and Dr. Antonia Gentile for performing the histologic grading of liver biopsies.

GRANTS

This work was supported by Ministero dell'Università e della Ricerca, Italy, PRIN (to F. Giorgino).

DISCLOSURES

No conflicts of interest, financial or otherwise, are declared by the author(s).

AUTHOR CONTRIBUTIONS

Author contributions: S. Perrini, L.L., and F.G. conception and design of research; S. Perrini, F.T., A.N., A.C., A.L., R.F., T.M.C., and F.G. analyzed data; S. Perrini, F.T., A.N., A.L., T.M.C., L.L., G.P., and F.G. interpreted results of experiments; S. Perrini, F.T., and S. Porro prepared figures; S. Perrini drafted manuscript; S. Perrini, F.T., A.N., C.P., A.C., V.O.P., C.C., F.D.S., S. Porro, A.L., R.F., M.D.F., T.M.C., F.P., L.L., G.P., and F.G. approved final version of manuscript; F.T., C.P., V.O.P., C.C., F.D.S., S. Porro, R.F., M.D.F., and F.P. performed experiments; A.N., A.L., L.L., G.P., and F.G. edited and revised manuscript.

REFERENCES

1. **Almeida M, Han L, Ambrogini E, Bartell SM, Manolagas SC.** Oxidative stress stimulates apoptosis and activates NF-kappaB in osteoblastic cells via a PKCbeta/p66shc signaling cascade: counter regulation by estrogens or androgens. *Mol Endocrinol* 24: 2030–2037, 2010.
2. **Bataille AM, Manautou JE.** Nrf2: a potential target for new therapeutics in liver disease. *Clin Pharmacol Ther* 92: 340–348, 2012.
3. **Beltrami E, Ruggiero A, Busuttil R, Migliaccio E, Pelicci PG, Vijg J, Giorgio M.** Deletion of p66Shc in mice increases the frequency of size-change mutations in the lacZ transgene. *Aging Cell* 12: 177–183, 2013.
4. **Beyer TA, Xu W, Teupser D, auf dem Keller U, Bugnon P, Hildt E, Thiery J, Kan YW, Werner S.** Impaired liver regeneration in Nrf2 knockout mice: role of ROS-mediated insulin/IGF-1 resistance. *EMBO J* 27: 212–223, 2008.
5. **Cai C, Teng L, Vu D, He JQ, Guo Y, Li Q, Tang XL, Rokosh G, Bhatnagar A, Bolli R.** The heme oxygenase 1 inducer (CoPP) protects human cardiac stem cells against apoptosis through activation of the extracellular signal-regulated kinase (ERK)/NRF2 signaling pathway and cytokine release. *J Biol Chem* 287: 33720–33732, 2012.
6. **Chahdi A, Sorokin A.** Endothelin-1 induces p66Shc activation through EGF receptor transactivation: Role of beta(1)Pix/Galpha(i3) interaction. *Cell Signal* 22: 325–329, 2010.
7. **Cignarelli A, Melchiorre M, Peschechera A, Conserva A, Renna LA, Miccoli S, Natalicchio A, Perrini S, Laviola L, Giorgino F.** Role of UBC9 in the regulation of the adipogenic program in 3T3–L1 adipocytes. *Endocrinology* 151: 5255–5266, 2010.
8. **Clavel S, Siffroi-Fernandez S, Coldefy AS, Boulukos K, Pisani DF, Derijard B.** Regulation of the intracellular localization of Foxo3a by stress-activated protein kinase signaling pathways in skeletal muscle cells. *Mol Cell Biol* 30: 470–480, 2010.
9. **Colmenero J, Bataller R, Sancho-Bru P, Bellot P, Miquel R, Moreno M, Jares P, Bosch J, Arroyo V, Caballeria J, Gines P.** Hepatic expression of candidate genes in patients with alcoholic hepatitis: correlation with disease severity. *Gastroenterology* 132: 687–697, 2007.
10. **Giorgio M, Migliaccio E, Orsini F, Paolucci D, Moroni M, Contursi C, Pelliccia G, Luzi L, Minucci S, Marcaccio M, Pinton P, Rizzuto R, Bernardi P, Paolucci F, Pelicci PG.** Electron transfer between cytochrome c and p66Shc generates reactive oxygen species that trigger mitochondrial apoptosis. *Cell* 122: 221–233, 2005.
11. **Guo J, Gertsberg Z, Ozgen N, Steinberg SF.** p66Shc links alpha1-adrenergic receptors to a reactive oxygen species-dependent AKT-FOXO3A phosphorylation pathway in cardiomyocytes. *Circ Res* 104: 660–669, 2009.
12. **Haga S, Morita N, Irani K, Fujiyoshi M, Ogino T, Ozawa T, Ozaki M.** p66(Shc) has a pivotal function in impaired liver regeneration in aged mice by a redox-dependent mechanism. *Lab Invest* 90: 1718–1726, 2010.
13. **Haga S, Terui K, Fukai M, Oikawa Y, Irani K, Furukawa H, Todo S, Ozaki M.** Preventing hypoxia/reoxygenation damage to hepatocytes by

p66(shc) ablation: up-regulation of anti-oxidant and anti-apoptotic proteins. *J Hepatol* 48: 422–432, 2008.
14. **He X, Kan H, Cai L, Ma Q.** Nrf2 is critical in defense against high glucose-induced oxidative damage in cardiomyocytes. *J Mol Cell Cardiol* 46: 47–58, 2009.
15. **Huang XS, Chen HP, Yu HH, Yan YF, Liao ZP, Huang QR.** Nrf2-dependent upregulation of antioxidative enzymes: a novel pathway for hypoxic preconditioning-mediated delayed cardioprotection. *Mol Cell Biochem* 385: 33–41, 2014.
16. **Jackson JG, Yoneda T, Clark GM, Yee D.** Elevated levels of p66 Shc are found in breast cancer cell lines and primary tumors with high metastatic potential. *Clin Cancer Res* 6: 1135–1139, 2000.
17. **Koch OR, Fusco S, Ranieri SC, Maulucci G, Palozza P, Larocca LM, Cravero AA, Farre' SM, De Spirito M, Galeotti T, Pani G.** Role of the life span determinant P66(shcA) in ethanol-induced liver damage. *Lab Invest* 88: 750–760, 2008.
18. **Laviola L, Orlando MR, Incalza MA, Caccioppoli C, Melchiorre M, Leonardini A, Cignarelli A, Tortosa F, Labarbuta R, Martemucci S, Pacelli C, Cocco T, Perrini S, Natalicchio A, Giorgino F.** TNFα signals via p66(Shc) to induce E-selectin, promote leukocyte transmigration and enhance permeability in human endothelial cells. *PLoS One* 8: e81930, 2013.
19. **Menini S, Amadio L, Oddi G, Ricci C, Pesce C, Pugliese F, Giorgio M, Migliaccio E, Pelicci P, Iacobini C, Pugliese G.** Deletion of p66Shc longevity gene protects against experimental diabetic glomerulopathy by preventing diabetes-induced oxidative stress. *Diabetes* 55: 1642–1650, 2006.
20. **Michalak S, Rousselet MC, Bedossa P, Pilette C, Chappard D, Oberti F, Gallois Y, Cales P.** Respective roles of porto-septal fibrosis and centrilobular fibrosis in alcoholic liver disease. *J Pathol* 201: 55–62, 2003.
21. **Migliaccio E, Giorgio M, Mele S, Pelicci G, Reboldi P, Pandolfi PP, Lanfrancone L, Pelicci PG.** The p66shc adaptor protein controls oxidative stress response and life span in mammals. *Nature* 402: 309–313, 1999.
22. **Morita M, Matsuzaki H, Yamamoto T, Fukami Y, Kikkawa U.** Epidermal growth factor receptor phosphorylates protein kinase C-delta at Tyr332 to form a trimeric complex with p66Shc in the H_2O_2-stimulated cells. *J Biochem* 143: 31–38, 2008.
23. **Natalicchio A, De Stefano F, Perrini S, Laviola L, Cignarelli A, Caccioppoli C, Quagliara A, Melchiorre M, Leonardini A, Conserva A, Giorgino F.** Involvement of the p66Shc protein in glucose transport regulation in skeletal muscle myoblasts. *Am J Physiol Endocrinol Metab* 296: E228–E237, 2009.
24. **Okuda M, Li K, Beard MR, Showalter LA, Scholle F, Lemon SM, Weinman SA.** Mitochondrial injury, oxidative stress, and antioxidant gene expression are induced by hepatitis C virus core protein. *Gastroenterology* 122: 366–375, 2002.
25. **Pagnin E, Fadini G, de Toni R, Tiengo A, Calo L, Avogaro A.** Diabetes induces p66shc gene expression in human peripheral blood mononuclear cells: relationship to oxidative stress. *J Clin Endocrinol Metab* 90: 1130–1136, 2005.
26. **Polytarchou C, Pfau R, Hatziapostolou M, Tsichlis PN.** The JmjC domain histone demethylase Ndy1 regulates redox homeostasis and protects cells from oxidative stress. *Mol Cell Biol* 28: 7451–7464, 2008.
27. **Reid AE.** Nonalcoholic steatohepatitis. *Gastroenterology* 121: 710–723, 2001.
28. **Rota M, LeCapitaine N, Hosoda T, Boni A, De Angelis A, Padin-Iruegas ME, Esposito G, Vitale S, Urbanek K, Casarsa C, Giorgio M, Luscher TF, Pelicci PG, Anversa P, Leri A, Kajstura J.** Diabetes promotes cardiac stem cell aging and heart failure, which are prevented by deletion of the p66shc gene. *Circ Res* 99: 42–52, 2006.
29. **Sun L, Xiao L, Nie J, Liu FY, Ling GH, Zhu XJ, Tang WB, Chen WC, Xia YC, Zhan M, Ma MM, Peng YM, Liu H, Liu YH, Kanwar YS.** p66Shc mediates high-glucose and angiotensin II-induced oxidative stress renal tubular injury via mitochondrial-dependent apoptotic pathway. *Am J Physiol Renal Physiol* 299: F1014–F1025, 2010.
30. **Thannickal VJ, Fanburg BL.** Reactive oxygen species in cell signaling. *Am J Physiol Lung Cell Mol Physiol* 279: L1005–L1028, 2000.
31. **Tomita K, Teratani T, Suzuki T, Oshikawa T, Yokoyama H, Shimamura K, Nishiyama K, Mataki N, Irie R, Minamino T, Okada Y, Kurihara C, Ebinuma H, Saito H, Shimizu I, Yoshida Y, Hokari R, Sugiyama K, Hatsuse K, Yamamoto J, Kanai T, Miura S, Hibi T.** p53/p66Shc-mediated signaling contributes to the progression of non-alcoholic steatohepatitis in humans and mice. *J Hepatol* 57: 837–843, 2012.
32. **Trinei M, Giorgio M, Cicalese A, Barozzi S, Ventura A, Migliaccio E, Milia E, Padura IM, Raker VA, Maccarana M, Petronilli V, Minucci S, Bernardi P, Lanfrancone L, Pelicci PG.** A p53-p66Shc signalling pathway controls intracellular redox status, levels of oxidation-damaged DNA and oxidative stress-induced apoptosis. *Oncogene* 21: 3872–3878, 2002.
33. **Veal EA, Day AM, Morgan BA.** Hydrogen peroxide sensing and signaling. *Mol Cell* 26: 1–14, 2007.
34. **Veeramani S, Igawa T, Yuan TC, Lin FF, Lee MS, Lin JS, Johansson SL, Lin MF.** Expression of p66(Shc) protein correlates with proliferation of human prostate cancer cells. *Oncogene* 24: 7203–7212, 2005.
35. **Wang Z, Dou X, Li S, Zhang X, Sun X, Zhou Z, Song Z.** Nuclear factor (erythroid-derived 2)-like 2 activation-induced hepatic very-low-density lipoprotein receptor overexpression in response to oxidative stress contributes to alcoholic liver disease in mice. *Hepatology* 59: 1381–1392, 2014.
36. **Zhou S, Chen HZ, Wan YZ, Zhang QJ, Wei YS, Huang S, Liu JJ, Lu YB, Zhang ZQ, Yang RF, Zhang R, Cai H, Liu DP, Liang CC.** Repression of P66Shc expression by SIRT1 contributes to the prevention of hyperglycemia-induced endothelial dysfunction. *Circ Res* 109: 639–648, 2011.